Tspan18 is a novel regulator of the Ca^{2+} channel Orai1 and von Willebrand factor release in endothelial cells

Peter J. Noy,[1] Rebecca L. Gavin,[1] Dario Colombo,[2] Elizabeth J. Haining,[2] Jasmeet S. Reyat,[1] Holly Payne,[2] Ina Thielmann,[3] Adam B. Lokman,[2] Georgiana Neag,[2] Jing Yang,[1] Tammy Lloyd,[1] Neale Harrison,[1] Victoria L. Heath,[2] Chris Gardiner,[4] Katharine M. Whitworth,[5] Joseph Robinson,[5] Chek Z. Koo,[1] Alessandro Di Maio,[1] Paul Harrison,[6,7] Steven P. Lee,[5] Francesco Michelangeli,[8] Neena Kalia,[2,9] G. Ed Rainger,[2] Bernhard Nieswandt,[3] Alexander Brill,[2,9,10] Steve P. Watson[2,9] and Michael G. Tomlinson[1,9]

[1]School of Biosciences, College of Life and Environmental Sciences, University of Birmingham, Birmingham, UK

[2]Institute of Cardiovascular Sciences, College of Medical and Dental Sciences, University of Birmingham, Birmingham, UK

[3]University Hospital Würzburg and Rudolf Virchow Center for Experimental Biomedicine, Würzburg, Germany

[4]Department of Haematology, University College London, London, UK

[5]Institute of Immunology and Immunotherapy, Cancer Immunology and Immunotherapy Centre, University of Birmingham, Birmingham, UK

[6]Scar Free Foundation for Burns Research, Queen Elizabeth Hospital Birmingham, University Hospitals Birmingham National Health Service (NHS) Foundation Trust, Birmingham, UK

[7]Institute of Inflammation and Ageing, University of Birmingham, Birmingham, UK

[8]Department of Biological Sciences, University of Chester, Chester, UK

[9]Centre of Membrane Proteins and Receptors (COMPARE), Universities of Birmingham and Nottingham, UK

[10]Department of Pathophysiology, Sechenov First Moscow State Medical University, Moscow, Russia

Running head: Tspan18 regulates Orai1 in endothelial cells

Correspondence: Michael G. Tomlinson, School of Biosciences, College of Life and Environmental Sciences, University of Birmingham, Birmingham B15 2TT, UK; e-mail m.g.tomlinson@bham.ac.uk.

Word count: 3641

Figure count: 8

Acknowledgments

We are grateful to Carl Blobel, Chris Bunce, Dean Kavanagh, Neil Morgan and Steve Publicover for their helpful comments on this project. We thank the Birmingham Biomedical Sciences Unit for maintaining mice, and the Birmingham Advanced Light Microscope Facility for imaging expertise. This work was funded by a British Heart Foundation Project Grant (PG/13/92/30587) to M.G.T. which supported P.J.N., Biotechnology and Biological Sciences Research Council PhD Studentships to M.G.T. which supported R.L.G. and E.J.H., British Heart Foundation PhD Studentships to M.G.T which supported D.C., J.S.R. and C.Z.K. (FS/05/048, FS/12/79/29871 and FS/18/9/33388), a British Heart Foundation Senior

Fellowship (FS/08/062/25797) to M.G.T. which also supported J.Y., a Biotechnology and Biological Sciences Research Council Project Grant (BB/P00783X/1) to M.G.T. which supported N.H. and a Medical Research Council New Investigator Award (RRAK10717) which supported M.G.T.

Abstract

Ca^{2+} entry via Orai1 store-operated Ca^{2+} channels in the plasma membrane is critical to cell function, and Orai1 loss causes severe immunodeficiency and developmental defects. The tetraspanins are a superfamily of transmembrane proteins that interact with specific 'partner proteins' and regulate their trafficking and clustering. The aim of this study was to functionally characterize tetraspanin Tspan18. We show that Tspan18 is expressed by endothelial cells at several-fold higher levels than most other cell types analyzed. Tspan18-knockdown primary human umbilical vein endothelial cells (HUVECs) have 55-70% decreased Ca^{2+} mobilization upon stimulation with the inflammatory mediators thrombin or histamine, similar to Orai1-knockdown. Tspan18 interacts with Orai1, and Orai1 cell surface localization is reduced by 70% in Tspan18-knockdown HUVECs. Tspan18 over-expression in lymphocyte model cell lines induces 20-fold activation of Ca^{2+}-responsive NFAT signaling, in an Orai1-dependent manner. Tspan18-knockout mice are viable. They lose on average 6-fold more blood in a tail-bleed assay. This is due to Tspan18 deficiency in non-hematopoietic cells, as assessed using chimeric mice. Tspan18-knockout mice have 60% reduced thrombus size in a deep vein thrombosis model, and 50% reduced platelet deposition following myocardial ischemia-reperfusion injury. Histamine- or thrombin-induced von Willebrand factor (VWF) release from HUVECs is reduced by 90% following Tspan18-knockdown, and histamine-induced increase of plasma VWF is reduced by 45% in Tspan18-knockout mice. These findings identify Tspan18 as a novel regulator of endothelial cell Orai1/Ca^{2+} signaling and VWF release in response to inflammatory stimuli.

Introduction

The tetraspanins are a superfamily of proteins containing four transmembrane regions that interact with and regulate the trafficking, lateral mobility and clustering of specific 'partner proteins'. These include signaling receptors, adhesion molecules and metalloproteinases[1-3]. Recently, the first crystal structure of a tetraspanin, CD81, demonstrated a cone-shaped structure with a cholesterol-binding cavity within the transmembranes[4]. Molecular dynamics simulations suggest that cholesterol removal causes a dramatic conformational change, whereby the main extracellular region swings upwards[4]. This raises the possibility that tetraspanins function as 'molecular switches' to regulate partner protein function via conformational change, and suggests that tetraspanins are viable future drug targets.

Tetraspanin Tspan18 was previously studied in chick embryos, in which it stabilizes expression of the homophilic adhesion molecule cadherin 6B to maintain adherens junctions between premigratory epithelial cranial neural crest cells[5,6]. Transcriptional Tspan18 downregulation is required for loss of cadherin 6B expression, breakdown of epithelial junctions and neural crest cell migration. However, Tspan18 knockdown has no major effect on chick embryonic development[5,6]. The function of Tspan18 in humans or mice remains unstudied.

Store-operated Ca^{2+} entry (SOCE) through the plasma membrane Ca^{2+} channel Orai1 is essential for the healthy function of most cell types[7]. Loss of SOCE results in severe immunodeficiency that requires a bone marrow transplant for survival. Further symptoms include ectodermal dysplasia and impaired development of skeletal muscle[7]. The process of SOCE is biphasic. This first step is initiated following the generation of the second messenger inositol trisphosphate (IP3) from upstream tyrosine kinase or G protein-coupled receptor signaling. IP3 induces the transient release of Ca^{2+} from endoplasmic reticulum (ER) stores via IP3 receptor channels[8]. Depletion of Ca^{2+} is detected by the ER-resident dimeric Ca^{2+}-sensor protein STIM1, which then undergoes a conformational change and interacts with Orai1 hexamers in the plasma membrane[9,10]. STIM1 binding induces Orai1 channel opening and clustering via a mechanism that is not fully understood, allowing Ca^{2+} entry across the plasma membrane[9,10]. The resulting increase in intracellular Ca^{2+} concentration is relatively large and sustained, sufficient to activate a variety of signalling proteins including the widely-expressed nuclear factor of activated T cells (NFAT) transcription factors[8].

Endothelial cells line all blood and lymphatic vessels and play a central role in hemostasis and in thrombo-inflammation, in which inflammatory cells contribute to thrombosis[11,12]. In the thrombo-inflammatory disease deep vein thrombosis, blood flow stagnation induced by prolonged immobility, for example, is the trigger for endothelial cells to exocytose Weibel-Palade storage bodies via a mechanism involving Ca^{2+} signaling[13,14]. This releases the multimeric glycoprotein von Willebrand factor (VWF) and the adhesion molecule P-selectin, which recruit platelets and leukocytes, respectively. VWF-bound platelets provide a pro-coagulant surface for activation of clotting factors and thrombin generation, neutrophils release neutrophil extracellular traps, and mast cells release endothelial-activating substances[15-17]. This series of thrombo-inflammatory events leads to formation of a blood clot which occludes the vein, and can cause death by pulmonary thromboembolism.

The aim of this study was to determine the function of tetraspanin Tspan18 in humans and mice. We found that Tspan18 is highly expressed by endothelial cells, interacts with Orai1 and is required for its cell surface expression and SOCE function. As a consequence, Tspan18-deficient endothelial cells have impaired Ca^{2+} mobilization and release of VWF

upon activation induced by inflammatory mediators, and Tspan18-knockout mice are protected from deep vein thrombosis and myocardial ischemia-reperfusion injury, and have defective hemostasis.

Methods

Ethics statement

Procedures in Birmingham were approved by the UK Home Office according to the Animals (Scientific Procedures) Act 1986, and those in Würzburg by the district government of Lower Frankonia (Bezirksregierung Unterfranken).

Mice

Tspan18$^{-/-}$ mice were generated by Genentech/Lexicon Pharmaceuticals on a mixed genetic background of 129/SvEvBrd and C57BL/6J[18]. They were purchased from the Mutant Mouse Regional Resource Centre and bred as heterozygotes to generate litter-matched Tspan18$^{-/-}$ and Tspan18$^{+/+}$ pairs. Radiation fetal liver chimeric mice were generated as described[19].

Antibodies

Anti-epitope tag antibodies were mouse anti-Myc 9B11 and rabbit anti-Myc 71D10 (Cell Signaling Technology), mouse anti-FLAG M2 and rabbit anti-FLAG (Sigma). Other antibodies were mouse anti-human calnexin AF18 (Abcam), rat anti-mouse CD16/32 (BioLegend), CD41 (eBioscience) and panendothelial cell antigen MECA-32 (BD Pharmingen), mouse anti-ERK1/2 and rabbit anti-phospho-ERK1/2 (Cell Signaling Technology) and rabbit anti-human VWF (GE Healthcare). Biotinylated isolectin GS-IB$_4$ glycoprotein was from ThermoFisher Scientific.

Expression constructs

The NFAT/AP1-luciferase transcriptional reporter construct was described previously[20,21]. pEF6/Myc-His (mock) and pEF6/Myc-His/lacZ were from Invitrogen. N-terminal FLAG-tagged tetraspanin constructs were generated in pEF6/Myc-His as described[22,23]. pcDNA3.1 Myc-His-tagged human Orai1 and MO70-FLAG-tagged human Orai1 E106Q were from Addgene[24] and the dominant-active calcineurin was as described[25].

Cell culture and transfections

Detailed information on cell cultures is provided in the *Online Supplemental Material*. Wild-type and IP3 receptor-deficient DT40 chicken B-cell lines[26], and Jurkat human T-cell line, were transfected by electroporation[21]. Human embryonic kidney (HEK)-293T (HEK-293 cells expressing the large T-antigen of simian virus 40) and the human HeLa epithelial cell line were transfected using polyethylenimine (Sigma)[27] and Lipofectamine 2000 (Invitrogen)[28], respectively. Human umbilical vein endothelial cells (HUVECs)[29] were transfected with 10 nM Silencer Select siRNA duplexes (Invitrogen) using Lipectamine RNAiMAX (Invitrogen).

Quantitative real-time polymerase chain reaction (PCR)

Quantitative real-time PCR was performed using TaqMan assays for Tspan18, Orai1, Orai2, Orai3, 18S and GAPDH[30]. Detailed information is in *Online Supplemental Material*.

Lentiviral transduction

HUVECs were lentivirally transduced with Orai1-Myc as described[31]. Detailed information is in *Online Supplemental Material*.

NFAT/AP-1-luciferase transcriptional reporter assay

The NFAT/AP-1-luciferase assay, and β-galactosidase assay to normalize for transfection efficiency, were as described[21].

Co-immunoprecipitation

A detailed description of co-immunoprecipitation from transfected HEK-293T cell lysates[22] is provided in *Online Supplemental Material*.

Immunofluorescence microscopy

Detailed information is in *Online Supplemental Material*. In brief, cells were prepared as described[29] and the Manders coefficients (M1 and M2) were used as the colocalization measure[32]. Ear vasculature was imaged as described[33].

Immunohistochemistry

Immunohistochemistry was as described[34]; detailed information is in *Online Supplemental Material*.

Intracellular Ca^{2+}

HUVECs were loaded with Fluo-4 NW dye according to the manufacturer's instructions (Molecular Probes). Fluorescence was measured every 3 seconds for 5 minutes using a FlexStation fluorescence reader (Molecular Devices), and thrombin (1 U/ml), histamine (20 μM) or ionomycin (10 μM) were injected after acquiring a baseline for 30 seconds.

ELISA and coagulation time assays

Detailed information is in *Online Supplemental Material*.

Platelet aggregation and adhesion to HUVECs

Platelet assays were as described[35,36]; detailed information is in *Online Supplemental Material*.

In vivo assays

Mouse models were as described[13,36-38]; detailed information is in *Online Supplemental Material*.

Results

Tspan18 is expressed by endothelial cells

A lack of effective antibodies to many tetraspanins is a current problem in the tetraspanin field. This may be due to their relatively small size, high degree of sequence conservation during evolution and compact four-transmembrane structure[4]. For example, no Tspan18 antibodies have been published, and commercially-available antibodies are made to Tspan18 peptides and do not detect full-length Tspan18 when rigorously tested (Tomlinson M.G., unpublished). Therefore, to characterize the Tspan18 expression profile, mouse tissues were tested by quantitative real-time PCR. Tspan18 mRNA was most highly expressed in lung and at lower levels in other tissues (Figure 1A). Analyses of published transcriptomic data[39] showed that Tspan18 was most highly expressed by endothelial cells compared to other mouse lung cell types (Figure 1B). Similar analyses of transcriptomic data from mouse brain[40] also showed relatively strong endothelial expression of Tspan18 (Figure 1C). Consistent with this, quantitative real-time PCR showed that Tspan18 was expressed by primary human umbilical vein endothelial cells (HUVECs) and the human microvascular endothelial HMEC-1 cell line (Figure 1D). Tspan18 expression was low or absent on most other cell types tested, although peripheral blood leukocytes expressed comparable levels to HUVECs (Figure 1D). In transcriptomic data from the Human Protein Atlas (www.proteinatlas.org), Tspan18 was expressed by most human tissues at a level between 10 and 70 tags per million, but in cell lines was only expressed at 10 or greater tags per million by HUVECs and 8 of the other 64 cell types analyzed[41].

Tspan18 is required for Ca^{2+} signalling in primary human endothelial cells

To investigate Tspan18 function, its expression in HUVECs, which are a widely-used primary human endothelial cell model, was knocked down using two different siRNA duplexes. Subsequent analyses revealed a 60% reduction in peak Ca^{2+} elevation in response to the inflammatory mediator thrombin (Figure 2A). A similar defect was observed in response to histamine (Figure 2B). Positive control ionomycin treatment gave a sustained intracellular Ca^{2+} response in all samples (Figure 2C) and effective knockdown was confirmed by quantitative real-time PCR (Figure 2D). Functionality of thrombin and histamine receptors was confirmed by anti-phospho-ERK1/2 mitogen-activated protein kinase (MAPK) western blotting, as this was not affected by Tspan18 knockdown (Figure 2E).

Tspan18 promotes Ca^{2+}-responsive NFAT signalling in lymphocyte cell lines

To investigate the mechanism by which Tspan18 regulates Ca^{2+} signalling, a more tractable cell line system was established, namely DT40 cells that are derived from chicken B-cells. In this cell line, a transfected nuclear factor of activated T cells (NFAT)/adapter protein 1 (AP-1) transcriptional luciferase reporter can be used as a readout for Ca^{2+} signalling downstream of transfected membrane proteins[21,42]. Transfection of a FLAG epitope-tagged Tspan18 expression construct was sufficient to induce robust NFAT/AP-1 activation (Figure 3A). As controls, five other FLAG-tagged tetraspanins (CD9, CD63, CD151, Tspan32 and Tspan9) were chosen because they represent a diverse range of tetraspanins based on sequence identities[22]. These did not induce NFAT/AP-1 activation, despite their substantially higher expression than Tspan18 as assessed by anti-FLAG western blotting (Figure 3A).

Despite the fact that the NFAT/AP-1 promoter can be activated by Ca^{2+} signalling, it is maximally activated by combined Ca^{2+} signalling and MAPK; Ca^{2+} activates NFAT and MAPK activates AP-1. To determine whether Tspan18 activates Ca^{2+} signalling, MAPK or both, Tspan18-transfected DT40 cells were stimulated with the Ca^{2+} ionophore ionomycin or phorbol ester PMA to activate the MAPK pathway. PMA synergized with Tspan18 expression

in activating NFAT/AP-1, but ionomycin did not (Figure 3B). As a positive control, combined PMA and ionomycin induced relatively strong NFAT/AP-1 activation in the presence or absence of Tspan18 (Figure 3B). The capacity of Tspan18 over-expression to induce NFAT/AP-1 activation was not restricted to DT40 B-cells, since similar data were obtained in the human Jurkat T-cell line (Figure 3C). Taken together, these data suggest that Tspan18 promotes Ca^{2+} signalling and NFAT activation via a mechanism that is common to endothelial cells, B-cells and T-cells.

Tspan18-induced NFAT activation requires functional Orai1 SOCE channels

To understand the mechanism by which Tspan18 promotes Ca^{2+} signalling, a series of NFAT/AP-1 reporter experiments were conducted in gene-knockout DT40 cells and using inhibitors and a dominant-interfering construct. Firstly, Tspan18-induced NFAT/AP-1 activation was found to be independent of the three IP3 receptors (Figure 3D). IP3 receptors release Ca^{2+} from ER stores in response to tyrosine kinase and G protein-coupled receptor activation, suggesting that Tspan18 does not operate on these pathways or IP3 receptors themselves. However, Tspan18 did not activate NFAT/AP-1 following chelation of extracellular Ca^{2+} (Figure 3E), or following treatment with the immunosuppressive drug cyclosporin A (Figure 3F), which prevents NFAT translocation to the nucleus by inhibiting its activatory phosphatase calcineurin. These data suggest that Tspan18 might induce Ca^{2+} entry via the SOCE channel Orai1, a major entry route for extracellular Ca^{2+} in non-excitable cells[8]. Consistent with this possibility, a dominant interfering form of Orai1 (E106Q), which multimerizes with endogenous Orai1 to yield a non-functional channel[43-45], inhibited Tspan18-induced NFAT/AP-1 activation (Figure 3G). As a positive control to confirm that downstream NFAT signalling was still intact in the presence of dominant interfering Orai1, its inhibitory effect was overcome by the expression of an active form of calcineurin (Figure 3G). Therefore, Tspan18 may activate Ca^{2+} entry through the Orai1 SOCE pathway.

Tspan18 interacts with Orai1

To investigate whether Tspan18 interacts with Orai1, transfected epitope-tagged proteins were used because of the lack of effective antibodies to Tspan18. To test for an interaction using co-immunoprecipitation, transfected HEK-293T cells were lyzed in 1% digitonin, a stringent detergent that has been used previously to identify tetraspanin-partner protein interactions[22,46]. FLAG-tagged Tspan18 co-immunoprecipitated with Myc-tagged Orai1, but five other control tetraspanins did not (Figure 4A). Moreover, Tspan18 and Orai1 co-localized when expressed in HeLa cells, at a level of approximately 90% pixel co-localisation when assessed using the Manders' Coefficient (Figure 4B). These data suggest that Tspan18 interacts with Orai1.

Orai1-knockdown endothelial cells have impaired Ca^{2+} mobilization and Orai1 surface expression requires Tspan18

To determine whether knockdown of Orai1 could phenocopy Tspan18 knockdown, intracellular Ca^{2+} mobilisation was measured following siRNA-mediated knockdown of Orai1. This resulted in impaired Ca^{2+} mobilisation in response to thrombin (Figure 5A) or histamine (Figure 5B). As a control, knockdown of the other Orai family members, Orai2 and Orai3, did not affect Ca^{2+} mobilisation (Figures 5A-B), in agreement with previous studies on Orai proteins in HUVECs[47,48]. Positive control ionomycin treatment gave a sustained intracellular Ca^{2+} response in all samples (Figure 5C) and effective knockdown was confirmed by quantitative PCR (Figures 5D-F).

A common mechanism of tetraspanin function is to regulate their partner proteins by facilitating their exit from the endoplasmic reticulum (ER) and trafficking to the cell

surface[1,49,50]. To determine whether Orai1 localisation could be regulated by Tspan18 in this manner, HUVECs were lentivirally transduced with Myc-Orai1 and transfected with control or Tspan18 siRNA duplexes, and Orai1 subcellular localisation assessed by confocal microscopy. Orai1 was localized primarily to the cell periphery in control cells, but was this reduced following Tspan18 knockdown, with Orai1 strikingly co-localized with the ER marker calnexin (Figure 5G). Quantitative analyses showed that approximately 40% of Orai1 was ER-localized in Tspan18 knockdown cells compared to 10-15% in control cells (Figure 5G). These data support a role for Tspan18 in regulating Orai1 exit from the ER and trafficking to the cell surface.

Tspan18 deficient mice have impaired hemostasis due to a defect in non-haematopoietic cells

To investigate Tspan18 function *in vivo*, Tspan18-knockout mice were acquired from Genetech/Lexicon Pharmaceuticals. These mice had been generated as part of a library of 472 knockouts[18], but were functionally uncharacterized. Breeding of heterozygotes gave an equal proportion of male and female mice with Mendelian genotype ratios, and the mice bred successfully as homozygote knockouts (data not shown). Furthermore, Tspan18-knockout mice had normal body weights and whole blood cell counts (data not shown).

Tspan18-knockout mice were first evaluated for a hemostasis phenotype using a tail bleed assay. Most Tspan18-knockout mice bled more than wild-type littermates, demonstrating a significant disruption to hemostasis (Figure 6A). Some Tspan18-knockout mice did not bleed excessively (Figure 6A), indicating that the bleeding phenotype was variable. This variability could be due to genetic modifier loci, as demonstrated in mice deficient for the platelet collagen/fibrin receptor GPVI[51]. To determine whether impaired hemostasis was due to loss of Tspan18 from hematopoietic or non-hematopoietic cells, tail bleeding assays were performed on radiation fetal liver chimeric mice. These demonstrated that the bleeding phenotype was due to Tspan18 loss from non-hematopoietic cells (Figure 6A), and suggests that a platelet defect is not responsible. Consistent with this, Tspan18-knockout platelets aggregated normally in response to collagen (Figure 6B) or thrombin (Figure 6C). Furthermore, prothrombin time and activated partial thromboplastin time tests showed that coagulation was similar for wild-type and Tspan18-knockout plasma (Figures 6D-E). These data suggest that the impaired hemostasis phenotype is due to a defect in a non-hematopoietic vascular cell type such as the endothelial cell. This did not appear to be due to any observable structural defects in the vasculature, because immunohistochemistry analyses of blood vessels in organs such as kidney and pancreas were similar for wild-type and Tspan18-knockout mice (Figure 6F), as were immunofluorescence analyses of blood vessels in the ear (Figure 6G).

Tspan18 and Orai1 are required for endothelial release of VWF in response to inflammatory mediators

Endothelial cell stimulation by inflammatory agonists induces VWF release from Weibel-Palade bodies via a process that involves Ca^{2+} signalling[14]. To investigate whether Tspan18 could be required for VWF release, HUVECs were subjected to Tspan18 knockdown and stimulated in culture medium with thrombin or histamine. Soluble VWF release, as detected by ELISA, was reduced by approximately 90% compared to control cells (Figure 7A). This was corroborated by immunofluorescent staining of VWF that showed minimal release of Weibel-Palade bodies after Tspan18 knockdown (Figure 7B). Similar to Tspan18, Orai1 knockdown reduced Weibel-Palade body release after thrombin stimulation, but knockdown of Orai2 or Orai3 had no effect (Figure 7C). Furthermore, Tspan18 knockdown reduced platelet adhesion to a thrombin-activated HUVEC monolayer by 85-90% (Figure 7D). These

data support a role for Tspan18 and Orai1 in VWF release and platelet capture following endothelial cell activation by inflammatory mediators.

Tspan18-knockout mice have impaired histamine-induced release of endothelial VWF and impaired thombo-inflammatory responses

To determine whether Tspan18 has a role in VWF release *in vivo*, Tspan18-knockout mice were intra-peritoneally injected with histamine, and plasma VWF levels analyzed by ELISA. Induced plasma VWF release was reduced by approximately 50% in the absence of Tspan18 (Figure 8A). Basal plasma VWF was normal in Tspan18-knockout mice (Figure 8A), indicating a requirement for Tspan18 in regulated, but not basal, VWF release.

To investigate the role of Tspan18 in thrombosis, two arterial thrombosis models and two thrombo-inflammatory models were used. In a platelet-driven aorta injury arterial thrombosis model[37], no difference in time to complete occlusion of the vessel between Tspan18-knockout and wild-type littermate control mice was observed (Figure 8B). Similarly, there was no thrombosis defect in mesenteric arterioles following application of $FeCl_3$ (Figure 8C), which is also a platelet-driven model[37], but shows reduced platelet deposition and thrombus formation in the complete absence of VWF[52,53]. In a deep vein thrombosis thrombo-inflammatory model that is dependent on endothelial VWF[13], thrombus length and weight were reduced by approximately 60% in the Tspan18-knockout mice, compared to wild-type littermate controls (Figure 8D). Moreover, 4 out of 9 Tspan18-knockout mice failed to develop a thrombus compared to 100% thrombus formation in wild-type (Figure 8D). Macroscopically, thrombi from Tspan18-knockout mice had similar red and white parts to those from wild-type mice (data not shown). Finally, in a VWF-dependent myocardial ischemia-reperfusion thrombo-inflammatory model[54,55], platelet deposition and aggregate size were reduced by approximately 50% (Figure 8E). The reduction in severity in the two thrombo-inflammatory models is consistent with the requirement of Tspan18 for endothelial VWF release in response to inflammatory mediators.

Discussion

We have discovered that Tspan18 is expressed by endothelial cells and interacts with the SOCE channel Orai1. Tspan18-knockdown endothelial cells had reduced Orai1 expression at the cell surface and impaired Ca^{2+} signaling. This is consistent with the established role of tetraspanins in interacting with specific partner proteins in the endoplasmic reticulum, and promoting their trafficking to the cell surface[1,49,50], albeit via mechanisms that are yet to be defined. Tspan18 is not particularly related to any of the other 32 mammalian tetraspanins[22], suggesting that it may be unique amongst tetraspanins in regulating Orai1. Indeed, none of the five tetraspanins that were selected as controls interacted with Orai1, or induced Ca^{2+}-responsive NFAT activation, when over-expressed.

At the cell surface, tetraspanins can regulate the lateral diffusion and clustering of their partner proteins[2,3]. A question that arises from the present study is whether Tspan18 regulates Orai1 clustering at the endothelial cell surface. Interestingly, a unimolecular coupling model of Orai1 activation was recently proposed, whereby one molecule of a STIM1 dimer is sufficient to induce opening of the Orai1 hexamer channel[10]. This would enable the other STIM1 molecule in the dimer to cross-link with a second Orai1 hexamer and form a lattice of clustered Orai1 channels. The degree of cluster formation could dictate the kinetics of channel activation and could concentrate Ca^{2+} influx to particular regions of the plasma membrane[10]. This could affect the extent to which downstream effectors are activated. Tetraspanins have been reported to exist as nanodomains of approximately ten tetraspanins of a single type[56], therefore Tspan18 may cluster Orai1 into pre-formed nanodomains, so modulating Orai1 lattice formation by STIM1. This may provide a means by which endothelial cells fine-tune SOCE and downstream functional responses. It remains to be determined whether Tspan18 also regulates Orai2 and Orai3, but we found no role for these Orai family members in inflammatory mediator-induced HUVEC Ca^{2+} mobilization, consistent with other studies[47,48].

The inflammatory mediators thrombin and histamine activate G protein-coupled receptors to induce downstream Ca^{2+} mobilization and the release of VWF from Weibel-Palade bodies[14]. Consistent with impaired Ca^{2+} signaling, Tspan18-knockout endothelial cells had impaired inflammatory mediator-induced VWF release in vitro and in vivo. In contrast, basal release of VWF appeared to be normal, because basal plasma VWF levels were unaffected in Tspan18-knockout mice. We hypothesize that impaired VWF release, in response to inflammatory mediators, explains the in vivo phenotypes observed in Tspan18-knockout mice. The protection from deep vein thrombosis is consistent with the central role of VWF in this disease[13]. Furthermore, the reduced platelet deposition during myocardial ischemia-reperfusion injury is consistent with the role of VWF in this process[54,55]. The hemostasis defect cannot be explained at present, because although a tail bleeding phenotype has been demonstrated in endothelial-specific VWF-knockout mice, these animals also had low plasma VWF[57,58], unlike Tspan18 knockouts. The tail bleeding assay measures blood loss following excision of the tip of the tail, which contains the two lateral veins, the dorsal vein and the ventral artery. We speculate that endothelial cells in the veins and artery, adjacent to the site of excision, are activated and release VWF via Ca^{2+}-dependent signaling. The VWF may trap platelets, facilitating their aggregation and preventing excessive blood loss from the site of tail injury. Therefore, our data suggest that acute release of VWF adjacent to a site of injury might be important for hemostasis, at least for some types of injury. Finally, the lack of a phenotype in the two arterial thrombosis models is consistent with the importance of platelets in these models[37], and we found no defect in aggregation in vitro for Tspan18-knockout platelets.

In summary, we have identified Tspan18 as a novel regulator of endothelial Orai1 and SOCE. Our in vivo data show that Tspan18 regulates inflammation-induced VWF release but not basal release, and promotes hemostasis and thrombo-inflammatory processes but not arterial thrombosis.

References

1. Matthews AL, Szyroka J, Collier R, Noy PJ, Tomlinson MG. Scissor sisters: regulation of ADAM10 by the TspanC8 tetraspanins. Biochem Soc Trans. 2017;45(3):719-730.
2. Termini CM, Gillette JM. Tetraspanins Function as Regulators of Cellular Signaling. Front Cell Dev Biol. 2017;5:34.
3. van Deventer SJ, Dunlock VE, van Spriel AB. Molecular interactions shaping the tetraspanin web. Biochem Soc Trans. 2017;45(3):741-750.
4. Zimmerman B, Kelly B, McMillan BJ, Seegar TC, Dror RO, Kruse AC, et al. Crystal Structure of a Full-Length Human Tetraspanin Reveals a Cholesterol-Binding Pocket. Cell. 2016;167(4):1041-1051.
5. Fairchild CL, Conway JP, Schiffmacher AT, Taneyhill LA, Gammill LS. FoxD3 regulates cranial neural crest EMT via downregulation of tetraspanin18 independent of its functions during neural crest formation. Mechanisms of development. 2014;132:1-12.
6. Fairchild CL, Gammill LS. Tetraspanin18 is a FoxD3-responsive antagonist of cranial neural crest epithelial-to-mesenchymal transition that maintains cadherin-6B protein. J Cell Sci. 2013;126(Pt 6):1464-1476.
7. Putney JW, Steinckwich-Besancon N, Numaga-Tomita T, Davis FM, Desai PN, D'Agostin DM, et al. The functions of store-operated calcium channels. Biochim Biophys Acta. 2017;1864(6):900-906.
8. Trebak M, Putney JW, Jr. ORAI Calcium Channels. Physiology (Bethesda). 2017;32(4):332-342.
9. Yeung PS, Yamashita M, Prakriya M. Pore opening mechanism of CRAC channels. Cell Calcium. 2017;63:14-19.
10. Zhou Y, Cai X, Nwokonko RM, Loktionova NA, Wang Y, Gill DL. The STIM-Orai coupling interface and gating of the Orai1 channel. Cell Calcium. 2017;63:8-13.
11. Gragnano F, Sperlongano S, Golia E, Natale F, Bianchi R, Crisci M, et al. The Role of von Willebrand Factor in Vascular Inflammation: From Pathogenesis to Targeted Therapy. Mediators Inflamm. 2017;2017:5620314.
12. Kawecki C, Lenting PJ, Denis CV. von Willebrand factor and inflammation. J Thromb Haemost. 2017;15(7):1285-1294.
13. Brill A, Fuchs TA, Chauhan AK, Yang JJ, De Meyer SF, Kollnberger M, et al. von Willebrand factor-mediated platelet adhesion is critical for deep vein thrombosis in mouse models. Blood. 2011;117(4):1400-1407.
14. McCormack JJ, Lopes da Silva M, Ferraro F, Patella F, Cutler DF. Weibel-Palade bodies at a glance. J Cell Sci. 2017;130(21):3611-3617.
15. Brill A, Fuchs TA, Savchenko AS, Thomas GM, Martinod K, De Meyer SF, et al. Neutrophil extracellular traps promote deep vein thrombosis in mice. J Thromb Haemost. 2012;10(1):136-144.
16. Ponomaryov T, Payne H, Fabritz L, Wagner DD, Brill A. Mast Cells Granular Contents Are Crucial for Deep Vein Thrombosis in Mice. Circ Res. 2017;121(8):941-950.
17. von Bruhl ML, Stark K, Steinhart A, Chandraratne S, Konrad I, Lorenz M, et al. Monocytes, neutrophils, and platelets cooperate to initiate and propagate venous thrombosis in mice in vivo. J Exp Med. 2012;209(4):819-835.
18. Tang T, Li L, Tang J, Li Y, Lin WY, Martin F, et al. A mouse knockout library for secreted and transmembrane proteins. Nat Biotechnol. 2010;28(7):749-755.

19. Hughes CE, Navarro-Nunez L, Finney BA, Mourao-Sa D, Pollitt AY, Watson SP. CLEC-2 is not required for platelet aggregation at arteriolar shear. J Thromb Haemost. 2010;8(10):2328-2332.
20. Shapiro VS, Truitt KE, Imboden JB, Weiss A. CD28 mediates transcriptional upregulation of the interleukin-2 (IL-2) promoter through a composite element containing the CD28RE and NF-IL-2B AP-1 sites. Mol Cell Biol. 1997;17(7):4051-4058.
21. Tomlinson MG, Calaminus SD, Berlanga O, Auger JM, Bori-Sanz T, Meyaard L, et al. Collagen promotes sustained glycoprotein VI signaling in platelets and cell lines. J Thromb Haemost. 2007;5(11):2274-2283.
22. Haining EJ, Yang J, Bailey RL, Khan K, Collier R, Tsai S, et al. The TspanC8 subgroup of tetraspanins interacts with A disintegrin and metalloprotease 10 (ADAM10) and regulates its maturation and cell surface expression. J Biol Chem. 2012;287(47):39753-39765.
23. Protty MB, Watkins NA, Colombo D, Thomas SG, Heath VL, Herbert JM, et al. Identification of Tspan9 as a novel platelet tetraspanin and the collagen receptor GPVI as a component of tetraspanin microdomains. Biochem J. 2009;417(1):391-400.
24. Gwack Y, Srikanth S, Feske S, Cruz-Guilloty F, Oh-hora M, Neems DS, et al. Biochemical and functional characterization of Orai proteins. J Biol Chem. 2007;282(22):16232-16243.
25. O'Keefe SJ, Tamura J, Kincaid RL, Tocci MJ, O'Neill EA. FK-506- and CsA-sensitive activation of the interleukin-2 promoter by calcineurin. Nature. 1992;357(6380):692-694.
26. Sugawara H, Kurosaki M, Takata M, Kurosaki T. Genetic evidence for involvement of type 1, type 2 and type 3 inositol 1,4,5-trisphosphate receptors in signal transduction through the B-cell antigen receptor. Embo J. 1997;16(11):3078-3088.
27. Ehrhardt C, Schmolke M, Matzke A, Knoblauch A, Will C, Wixler V, et al. Polyethylenimine, a cost-effective transfection reagent. Signal Transduction. 2006;6:179–184.
28. Noy PJ, Yang J, Reyat JS, Matthews AL, Charlton AE, Furmston J, et al. TspanC8 Tetraspanins and A Disintegrin and Metalloprotease 10 (ADAM10) Interact via Their Extracellular Regions: EVIDENCE FOR DISTINCT BINDING MECHANISMS FOR DIFFERENT TspanC8 PROTEINS. J Biol Chem. 2016;291(7):3145-3157.
29. Wilson E, Leszczynska K, Poulter NS, Edelmann F, Salisbury VA, Noy PJ, et al. RhoJ interacts with the GIT-PIX complex and regulates focal adhesion disassembly. J Cell Sci. 2014;127(Pt 14):3039-3051.
30. Pfaffl MW. A new mathematical model for relative quantification in real-time RT-PCR. Nucleic Acids Res. 2001;29(9):e45.
31. Reyat JS, Tomlinson MG, Noy PJ. Utilizing Lentiviral Gene Transfer in Primary Endothelial Cells to Assess Lymphocyte-Endothelial Interactions. Methods Mol Biol. 2017;1591:155-168.
32. Manders EMM, Verbeek FJ, Aten JA. Measurement of Colocalization of Objects in Dual-Color Confocal Images. J Microsc-Oxford. 1993;169:375-382.
33. Gardenier JC, Hespe GE, Kataru RP, Savetsky IL, Torrisi JS, Nores GD, et al. Diphtheria toxin-mediated ablation of lymphatic endothelial cells results in progressive lymphedema. JCI Insight. 2016;1(15):e84095.
34. Parsonage G, Machado LR, Hui JW, McLarnon A, Schmaler T, Balasothy M, et al. CXCR6 and CCR5 localize T lymphocyte subsets in nasopharyngeal carcinoma. Am J Pathol. 2012;180(3):1215-1222.

35. Pollitt AY, Poulter NS, Gitz E, Navarro-Nunez L, Wang YJ, Hughes CE, et al. Syk and Src family kinases regulate C-type lectin receptor 2 (CLEC-2)-mediated clustering of podoplanin and platelet adhesion to lymphatic endothelial cells. J Biol Chem. 2014;289(52):35695-35710.
36. Senis YA, Tomlinson MG, Ellison S, Mazharian A, Lim J, Zhao Y, et al. The tyrosine phosphatase CD148 is an essential positive regulator of platelet activation and thrombosis. Blood. 2009;113:4942-4954.
37. Braun A, Varga-Szabo D, Kleinschnitz C, Pleines I, Bender M, Austinat M, et al. Orai1 (CRACM1) is the platelet SOC channel and essential for pathological thrombus formation. Blood. 2009;113(9):2056-2063.
38. Xu Z, Alloush J, Beck E, Weisleder N. A murine model of myocardial ischemia-reperfusion injury through ligation of the left anterior descending artery. J Vis Exp. 2014(86).
39. Du Y, Kitzmiller JA, Sridharan A, Perl AK, Bridges JP, Misra RS, et al. Lung Gene Expression Analysis (LGEA): an integrative web portal for comprehensive gene expression data analysis in lung development. Thorax. 2017;72(5):481-484.
40. Zhang Y, Chen K, Sloan SA, Bennett ML, Scholze AR, O'Keeffe S, et al. An RNA-sequencing transcriptome and splicing database of glia, neurons, and vascular cells of the cerebral cortex. The Journal of neuroscience : the official journal of the Society for Neuroscience. 2014;34(36):11929-11947.
41. Uhlen M, Fagerberg L, Hallstrom BM, Lindskog C, Oksvold P, Mardinoglu A, et al. Proteomics. Tissue-based map of the human proteome. Science. 2015;347(6220):1260419.
42. Fuller GL, Williams JA, Tomlinson MG, Eble JA, Hanna SL, Pohlmann S, et al. The C-type lectin receptors CLEC-2 and Dectin-1, but not DC-SIGN, signal via a novel YXXL-dependent signaling cascade. J Biol Chem. 2007;282(17):12397-12409.
43. Prakriya M, Feske S, Gwack Y, Srikanth S, Rao A, Hogan PG. Orai1 is an essential pore subunit of the CRAC channel. Nature. 2006;443(7108):230-233.
44. Vig M, Beck A, Billingsley JM, Lis A, Parvez S, Peinelt C, et al. CRACM1 multimers form the ion-selective pore of the CRAC channel. Curr Biol. 2006;16(20):2073-2079.
45. Yeromin AV, Zhang SL, Jiang W, Yu Y, Safrina O, Cahalan MD. Molecular identification of the CRAC channel by altered ion selectivity in a mutant of Orai. Nature. 2006;443(7108):226-229.
46. Dornier E, Coumailleau F, Ottavi JF, Moretti J, Boucheix C, Mauduit P, et al. TspanC8 tetraspanins regulate ADAM10/Kuzbanian trafficking and promote Notch activation in flies and mammals. J Cell Biol. 2012;199(3):481-496.
47. Li J, Cubbon RM, Wilson LA, Amer MS, McKeown L, Hou B, et al. Orai1 and CRAC channel dependence of VEGF-activated Ca2+ entry and endothelial tube formation. Circ Res. 2011;108(10):1190-1198.
48. Zhou MH, Zheng H, Si H, Jin Y, Peng JM, He L, et al. Stromal interaction molecule 1 (STIM1) and Orai1 mediate histamine-evoked calcium entry and nuclear factor of activated T-cells (NFAT) signaling in human umbilical vein endothelial cells. J Biol Chem. 2014;289(42):29446-29456.
49. Saint-Pol J, Eschenbrenner E, Dornier E, Boucheix C, Charrin S, Rubinstein E. Regulation of the trafficking and the function of the metalloprotease ADAM10 by tetraspanins. Biochem Soc Trans. 2017;45(4):937-944.
50. Vences-Catalan F, Duault C, Kuo CC, Rajapaksa R, Levy R, Levy S. CD81 as a tumor target. Biochem Soc Trans. 2017;45(2):531-535.

51. Cheli Y, Jensen D, Marchese P, Habart D, Wiltshire T, Cooke M, et al. The Modifier of hemostasis (Mh) locus on chromosome 4 controls in vivo hemostasis of Gp6-/- mice. Blood. 2008;111(3):1266-1273.
52. Denis C, Methia N, Frenette PS, Rayburn H, Ullman-Cullere M, Hynes RO, et al. A mouse model of severe von Willebrand disease: defects in hemostasis and thrombosis. Proc Natl Acad Sci U S A. 1998;95(16):9524-9529.
53. Ni H, Denis CV, Subbarao S, Degen JL, Sato TN, Hynes RO, et al. Persistence of platelet thrombus formation in arterioles of mice lacking both von Willebrand factor and fibrinogen. J Clin Invest. 2000;106(3):385-392.
54. De Meyer SF, Savchenko AS, Haas MS, Schatzberg D, Carroll MC, Schiviz A, et al. Protective anti-inflammatory effect of ADAMTS13 on myocardial ischemia/reperfusion injury in mice. Blood. 2012;120(26):5217-5223.
55. Gandhi C, Motto DG, Jensen M, Lentz SR, Chauhan AK. ADAMTS13 deficiency exacerbates VWF-dependent acute myocardial ischemia/reperfusion injury in mice. Blood. 2012;120(26):5224-5230.
56. Zuidscherwoude M, Gottfert F, Dunlock VM, Figdor CG, van den Bogaart G, van Spriel AB. The tetraspanin web revisited by super-resolution microscopy. Scientific reports. 2015;5:12201.
57. Kanaji S, Fahs SA, Shi Q, Haberichter SL, Montgomery RR. Contribution of platelet vs. endothelial VWF to platelet adhesion and hemostasis. J Thromb Haemost. 2012;10(8):1646-1652.
58. Verhenne S, Denorme F, Libbrecht S, Vandenbulcke A, Pareyn I, Deckmyn H, et al. Platelet-derived VWF is not essential for normal thrombosis and hemostasis but fosters ischemic stroke injury in mice. Blood. 2015;126(14):1715-1722.

Figures with Figure Legends

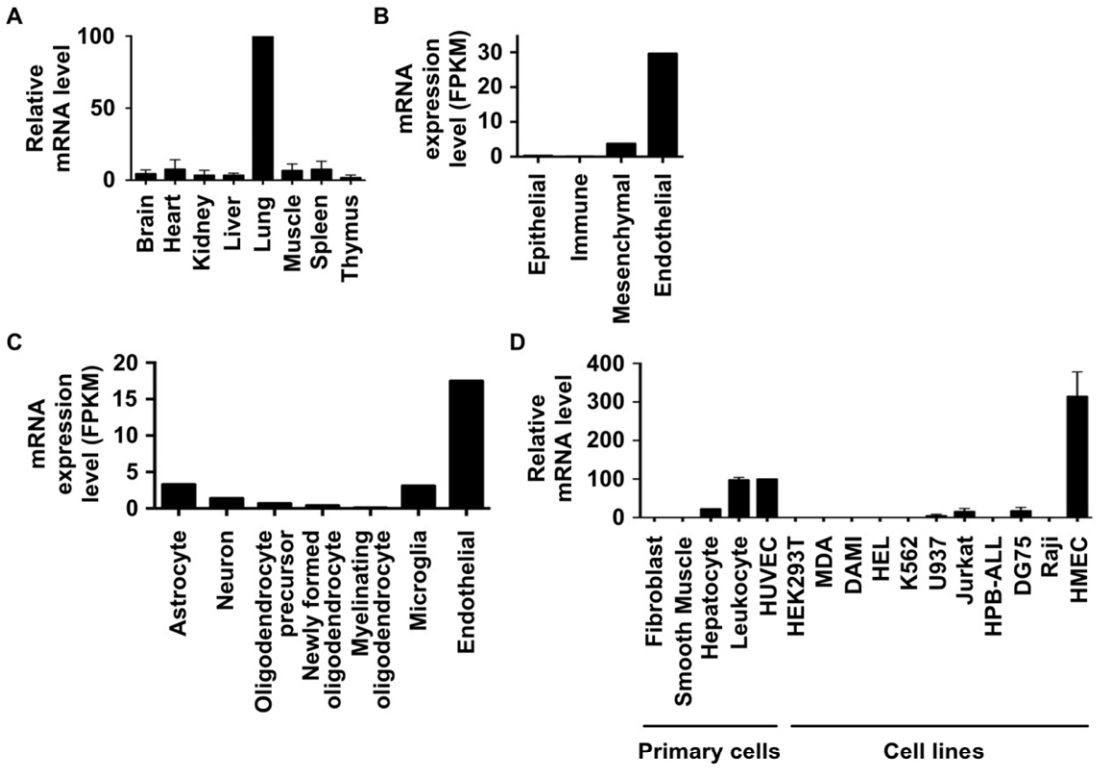

Figure 1. Tspan18 is highly expressed by endothelial cells and Tspan18-knockdown endothelial cells have impaired Ca^{2+} mobilization. (A) Quantitative real-time PCR was carried out for Tspan18 using cDNA derived from a panel of mouse tissues. Data were normalized for the HPRT housekeeping gene and adjusted such that the lung value was 100 in each experiment. Error bars represent standard error of the mean from three independent tissue samples. (B) RNA-Seq data from major cell types in mouse lung, generated by Du et al[39], was used to show Tspan18 mRNA expression levels as fragments per kilobase of transcript sequence per million mapped fragments (FPKM). (C) RNA-Seq data from major cell types in mouse brain, generated by Zhang et al[40], was used to show Tspan18 mRNA expression levels as described in panel B. (D) Quantitative real-time PCR was carried out for Tspan18 on cDNA derived from a panel of primary human cells (dermal fibroblasts, aortic smooth muscle, hepatocytes, peripheral blood leukocytes from buffy coat and HUVEC umbilical vein endothelial cells), and human cell lines (HEK-293T human embryonic kidney cells, MDA-MB-231 epithelial cells, DAMI megakaryocytic cells, HEL and K562 erythroleukemia cells, U937 monocytic cells, Jurkat and HPB-ALL T cells, DG75 and Raji B cells and HMEC-1 microvascular endothelial cells). Data were normalized for actin and adjusted such that the HUVEC value was 100 in each experiment. Error bars represent standard error of the mean from two independent cell samples.

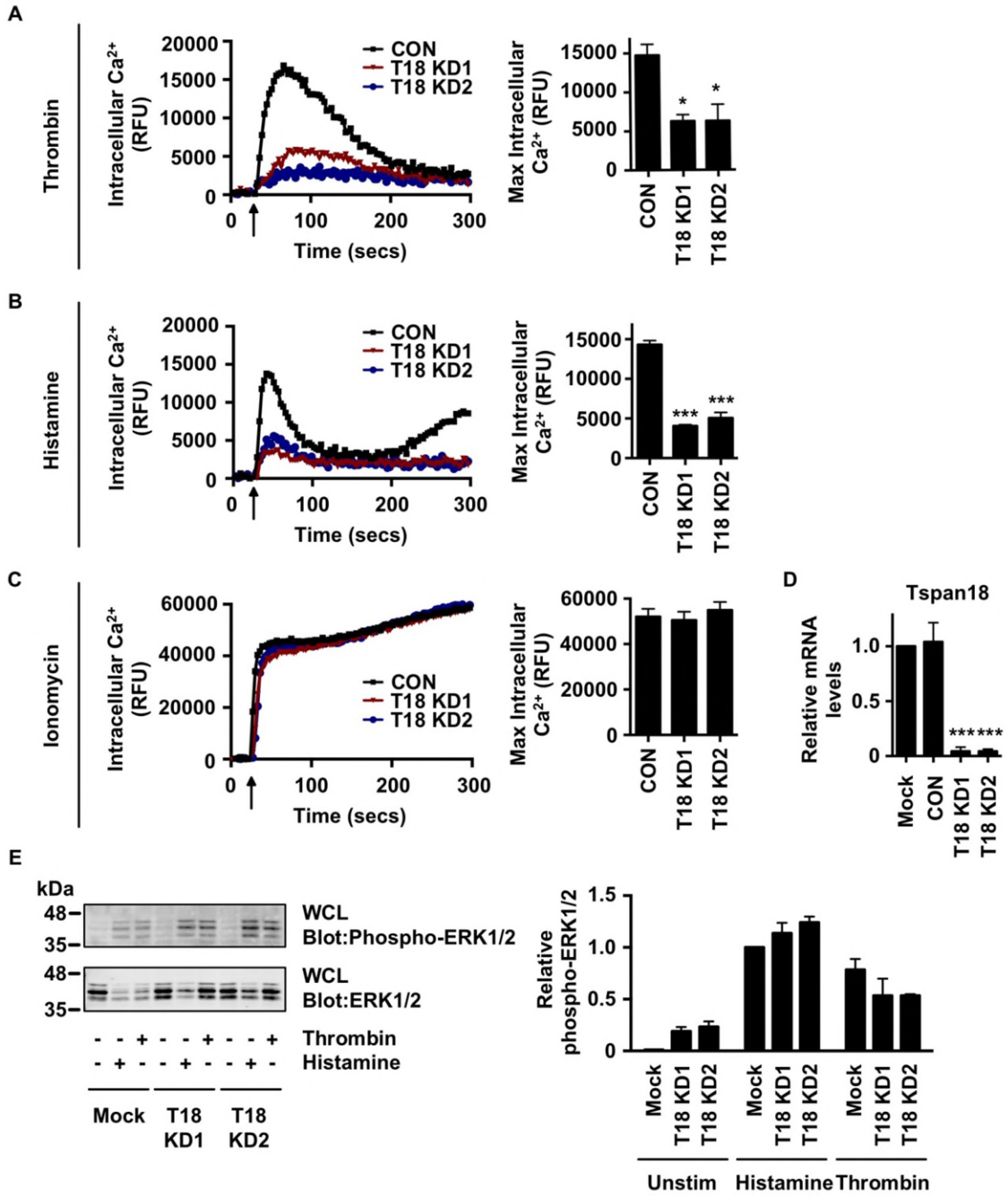

Figure 2. Tspan18-knockdown endothelial cells have impaired Ca^{2+} mobilization. (A-D) HUVECs were transfected with a negative control siRNA (CON) or with one of two independent siRNAs targeting Tspan18 (T18 KD). 48 hours later, HUVECs were loaded with the Ca^{2+}-sensitive dye Fluo-4 NW and Ca^{2+} measurements taken using a FlexStation fluorescence reader during addition (arrow) of (A) 1 U/ml thrombin, (B) 20 μM histamine, or (C) 10 μM ionomycin. Representative Ca^{2+} traces are shown for Tspan18-knockdown HUVECs (left panels), with quantitation of maximum intracellular Ca^{2+} concentrations (right panels). Data were analyzed by one-way ANOVA with Dunnett's multiple comparisons test. Error bars represent the standard error of the mean from three independent experiments (*P<0.05 and ***P<0.001). (D) siRNA-transfected HUVECs from panels A-B were

harvested, mRNA extracted, cDNA produced and Tspan18 mRNA levels were assessed by quantitative real-time PCR. Data were normalized to 18S and actin as internal controls and adjusted such that the non-siRNA-transfected mock value was 1 in each experiment. Data were then normalized by logarithmic transformation, and analyzed by one-way ANOVA and Tukey's multiple comparison test. Error bars represent the standard error of the mean from three independent experiments (***P<0.001). (E) HUVECs were subjected to Tspan18 siRNA knockdown as described for panels A-D, stimulated with 1 U/ml thrombin or 20 μM histamine for 5 minutes, then whole cell lysates were analyzed by western blotting with phospho-ERK1/2 and total ERK1/2 antibodies. Representative blots are shown in the left panel and quantitation of three independent experiments is shown on the right. Error bars represent standard error of the mean. Knockdown efficiency was similar to that shown in panel D (data not shown).

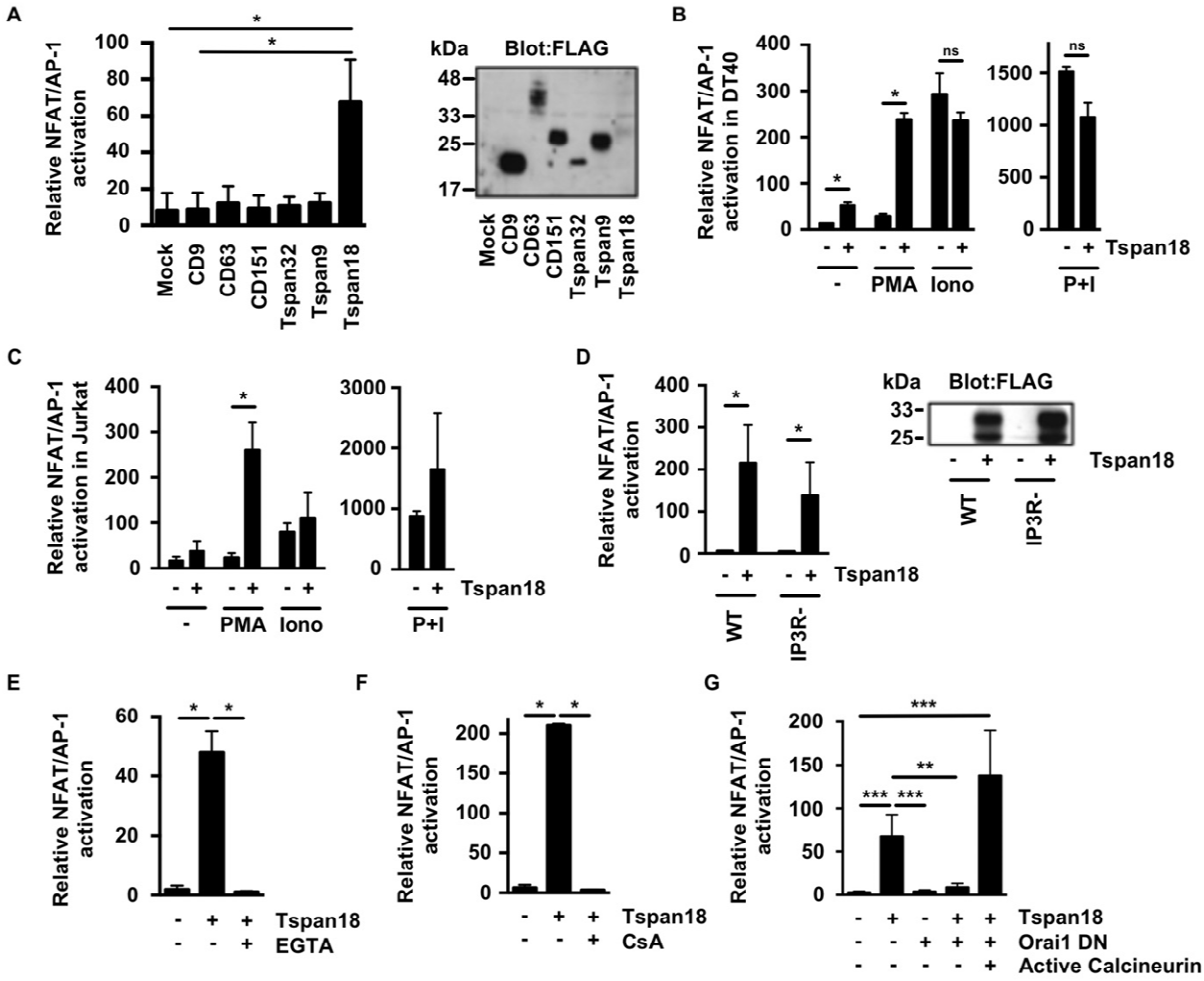
A
Relative NFAT/AP-1 activation
Mock
CD9
CD63
CD151
Tspan32
Tspan9
Tspan18
kDa
Blot:FLAG
48
33
25
17
B
Relative NFAT/AP-1 activation in DT40
ns
PMA
Iono
P+I
Tspan18
C
Relative NFAT/AP-1 activation in Jurkat
D
Relative NFAT/AP-1 activation
WT
IP3R-
E
EGTA
F
CsA
G
Orai1 DN
Active Calcineurin

Figure 3. Tspan18 over-expression in cell lines activates Ca^{2+}-responsive NFAT signalling in an Orai1-dependant manner. (A) The DT40 B cell line was transfected with an NFAT/AP-1-luciferase reporter construct, a β-galactosidase expression construct driven by the elongation factor (EF)-1α promoter to control for transfection efficiency, and FLAG-tagged mouse tetraspanin constructs or empty vector control. 24 hours post-transfection, cells were lyzed and assayed for luciferase and β-galactosidase. Luciferase data were normalized for β-galactosidase values (left panel). Whole cell lysates from these cells were separated by SDS-PAGE and blotted with an anti-FLAG antibody. A representative blot is shown (right panel). (B-C) The DT40 B cell line (B) and the human Jurkat T cell line (C) were transfected with an NFAT/AP-1-luciferase reporter construct and β-galactosidase expression construct with (+) or without (-) FLAG-tagged mouse Tspan18. 24 hours post-transfection cells were stimulated for six hours with 50 nM PMA or 1 μM ionomycin (Iono) (left panels), or both together (right panels). Luciferase assays were then performed as described in panel A. (D) DT40 cells with (+) or without (-) expression of FLAG-tagged mouse Tspan18 were tested for NFAT/AP-1 luciferase activity as described in panel A, but using cells with gene knockouts of the three IP_3 receptors (IP_3R^-) in comparison to wild-type (WT) cells (left panel). Whole cell lysates were western blotted with an anti-FLAG antibody (right panel). (E-F) DT40 cells with (+) or without (-) expression of FLAG-tagged mouse Tspan18 were tested for NFAT/AP-1 luciferase activity as described in panel A, except that cells were treated with 4 mM EGTA as a Ca^{2+} chelator (E) or with 2 mM cyclosporin A as a calcineurin inhibitor (F). (G) DT40 cells were transfected with FLAG-tagged human Tspan18 in the presence or absence of a dominant negative human Orai1 E106Q mutant construct, or a consitutively active human calcineurin construct. The experiment was conducted as described in panel A. All luciferase data were corrected for β-galactosidase values, normalized by logarithmic transformation, and analyzed by one-way ANOVA and Tukey's multiple comparison test (*P<0.05, **P<0.01 and ***P<0.001). Error bars represent the standard error of the mean from at least three independent experiments.

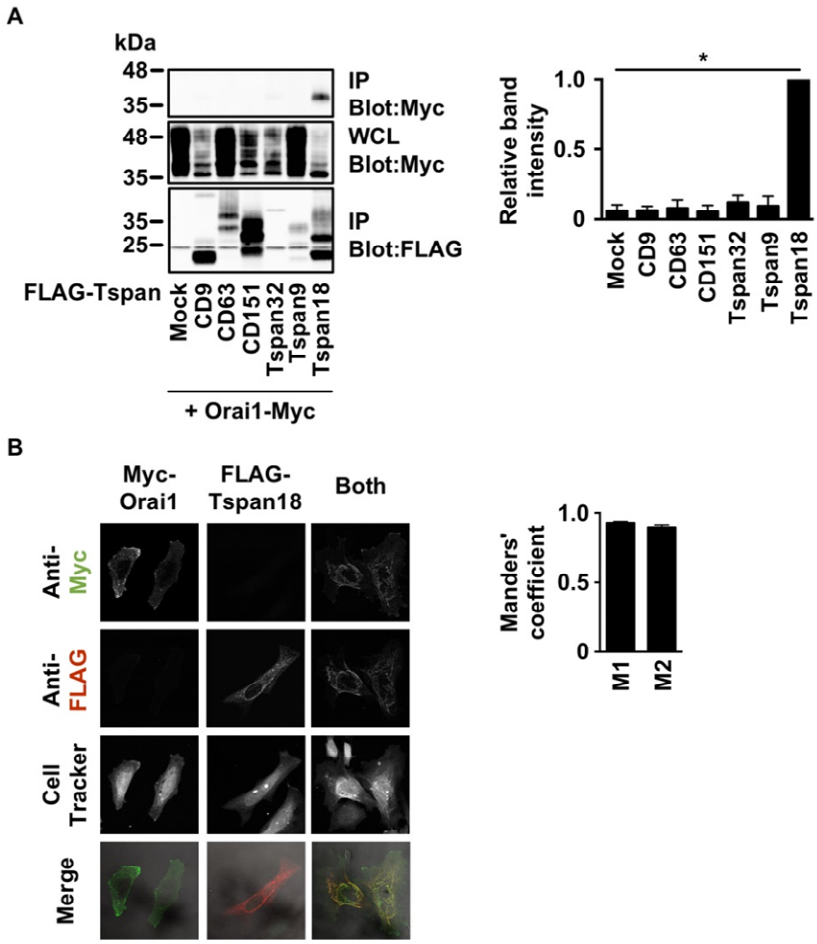

Figure 4. Tspan18 interacts with Orai1. (A) HEK-293T cells were tranfected with a Myc-tagged human Orai1 expression construct and one of a panel of FLAG-tagged human tetraspanin constructs. Cells were lyzed in 1% digitonin and immunoprecipitated with an anti-FLAG antibody. Samples were seperated by SDS-PAGE and both immunoprecipitated (i.p.) and whole call lysate (wcl) samples were blotted with anti-FLAG and anti-Myc antibodies. A representative blot for each is shown (left panel) with quantitation of Myc-tagged Orai1 immunoprecipitated with the tetraspanins (right panel). Data were nomalized by logarithmic transformation before analysis by one-way ANOVA and Dunnet's post-test. Error bars represent standard error of the mean from three independent experiments (*P<0.05). (B) HeLa cells were transfected with Myc-tagged human Orai1, FLAG-tagged human Tspan18, or both constructs. Cells were fixed and stained with an anti-Myc antibody (green), an anti-FLAG antibody (red) and imaged by confocal microscopy (left panels). The Manders coefficients (M1 and M2) were calculated from the confocal stacks to quantify the degree of overlap (right panel). Error bars represent the standard error of the mean from three independent experiments.

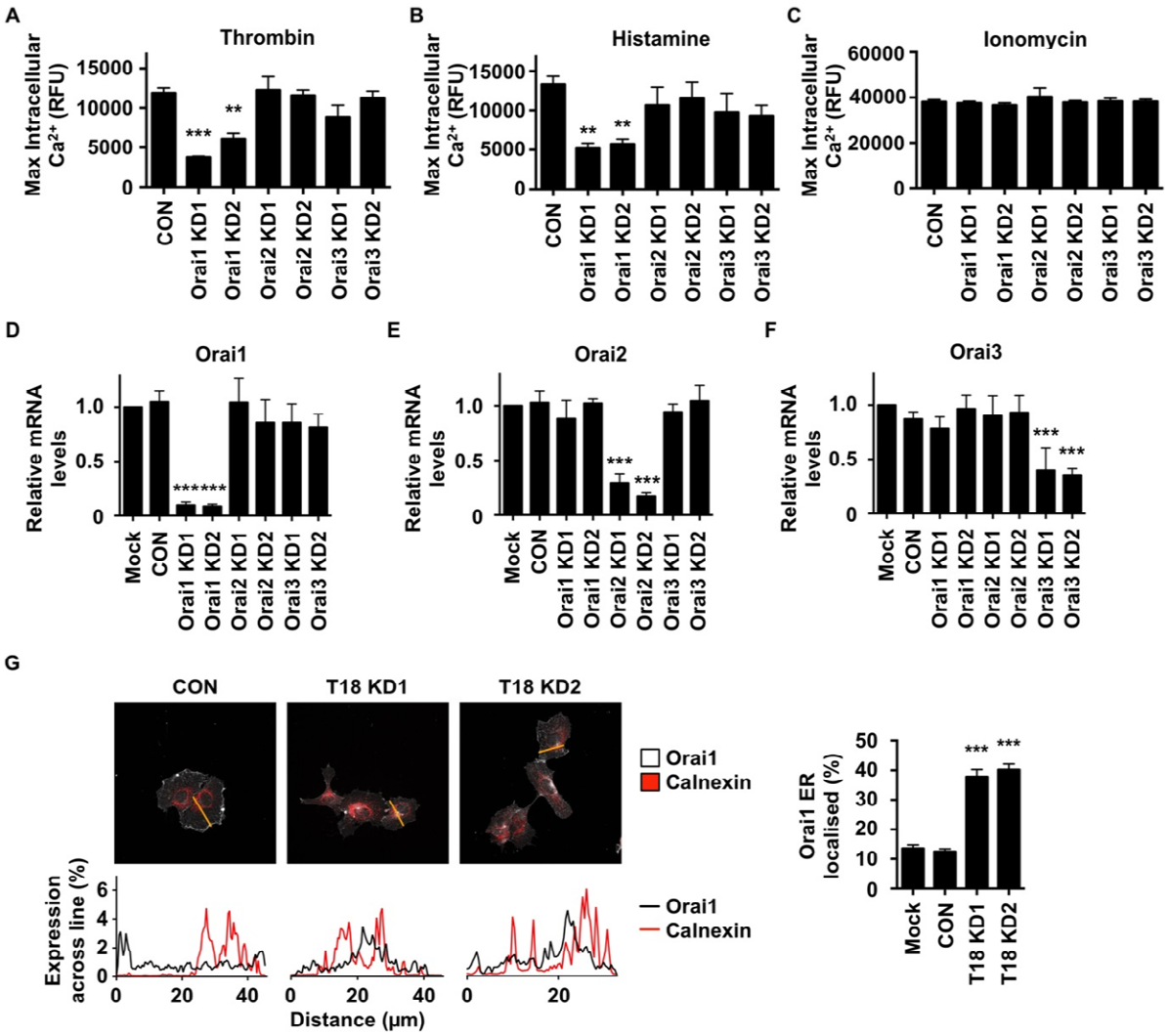

Figure 5. Orai1-knockdown endothelial cells have impaired Ca^{2+} mobilization and Orai1 surface expression requires Tspan18. (A-F) HUVECs were transfected with a negative control siRNA (CON) or with one of two independent siRNAs targeting Orai1, Orai2 or Orai3 (Orai1-3 KD). 48 hours later, Ca^{2+} measurements were taken as described in Figure 1E-G, following addition of 1 U/ml thrombin (A), 20 μM histamine (B), or 10 μM ionomycin (C), and quantitation of maximum intracellular Ca^{2+} concentrations is shown. Error bars represent standard error of the mean from three independent experiments (**P<0.01 and ***P<0.001). (D-F) siRNA-transfected HUVECs from panels A-C were subjected to quantitative real-time PCR for Orai1 (D), Orai2 (E) or Orai3 (F) as described for Figure 1H. Error bars represent standard error of the mean from three independent experiments (***P<0.001). (G) HUVECs lentivirally-transduced to express Myc-tagged Orai1 were treated with control or Tspan18 siRNAs. Cells were stained with anti-Myc (white) or anti-calnexin endoplasmic reticulum marker (red) antibodies and representative confocal microscopy images shown (upper panels). In the line graphs below the images (lower panels), the percentage expression of Orai1 (black) and calnexin (red) across the yellow line in the upper panel was determined using ImageJ. The percentage of Orai1 that localized to a calnexin endoplasmic reticulum mask was then quantified (right panel). Data were generated from 15 cells per condition from three independent experiments (five cells per condition per experiment). Error bars represent the standard error of the mean (***P<0.001).

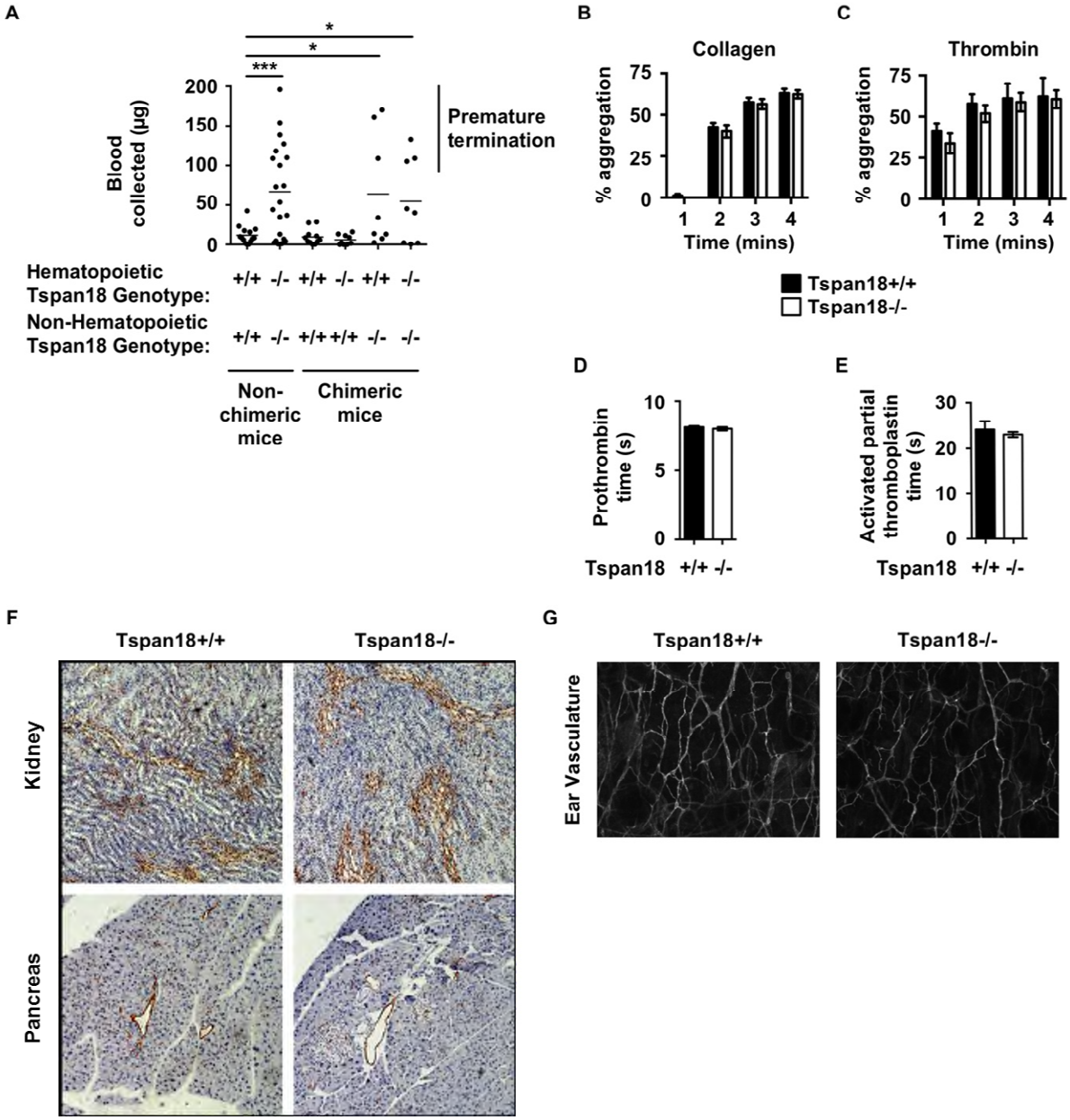

Figure 6. Tspan18-knockout mice have a hemostasis defect due to the absence of Tspan18 expression by non-hematopoietic cells. (A) Tail bleeding assays were done by amputating 3 mm tail tips of anaesthetized mice and the weight of blood lost was measured. The mice were Tspan18$^{+/+}$, Tspan18$^{-/-}$, or lethally irradiated Tspan18$^{-/-}$ or Tspan18$^{+/+}$ mice reconstituted with fetal liver cells from Tspan18$^{+/+}$ or Tspan18$^{-/-}$ embryos. Each symbol represents one animal. All data were analyzed by Fisher's exact test (*P<0.05 and ***P<0.001). Note that bleeding was stopped by cauterizing the tails of some mice, because of regulations limiting the amount of blood loss on our Home Office License. (B-C) Washed platelets from Tspan18$^{+/+}$ or Tspan18$^{-/-}$ mice were activated with 3 µg/ml collagen (B) or 0.3 U/ml thrombin (C), and aggregation was measured by light transmission with stirring. Quantitated percentage aggregation each minute is shown. Error bars represent the standard error of the mean from at least three pairs of litter-matched mice. (D-E) Plasma samples from Tspan18$^{+/+}$ and Tspan18$^{-/-}$ mice were subjected to a prothrombin time test with human placental thromboplastin (D) and an activated partial thromboplastin time test with purified

soy phosphatides with ellagic acid (E). Error bars represent the standard error of the mean from four pairs of litter-matched mice. (F) Immunohistochemistry was used to show a grossly normal vasculature in Tspan18$^{+/+}$ and Tspan18$^{-/-}$ mice formalin-fixed paraffin-embedded 5 μm sections from kidney and pancreas, using the MECA32 anti-mouse panendothelial cell antibody. Images are representative of three pairs of litter-matched mice. (G) Confocal microscopy was used to show a grossly normal vasculature in Tspan18$^{+/+}$ and Tspan18$^{-/-}$ mice ears, by staining anterior ear tissue with biotinylated isolectin GS-IB$_4$ glycoprotein followed by Alexa647-conjugated streptavidin. Images are representative of three pairs of litter-matched mice.

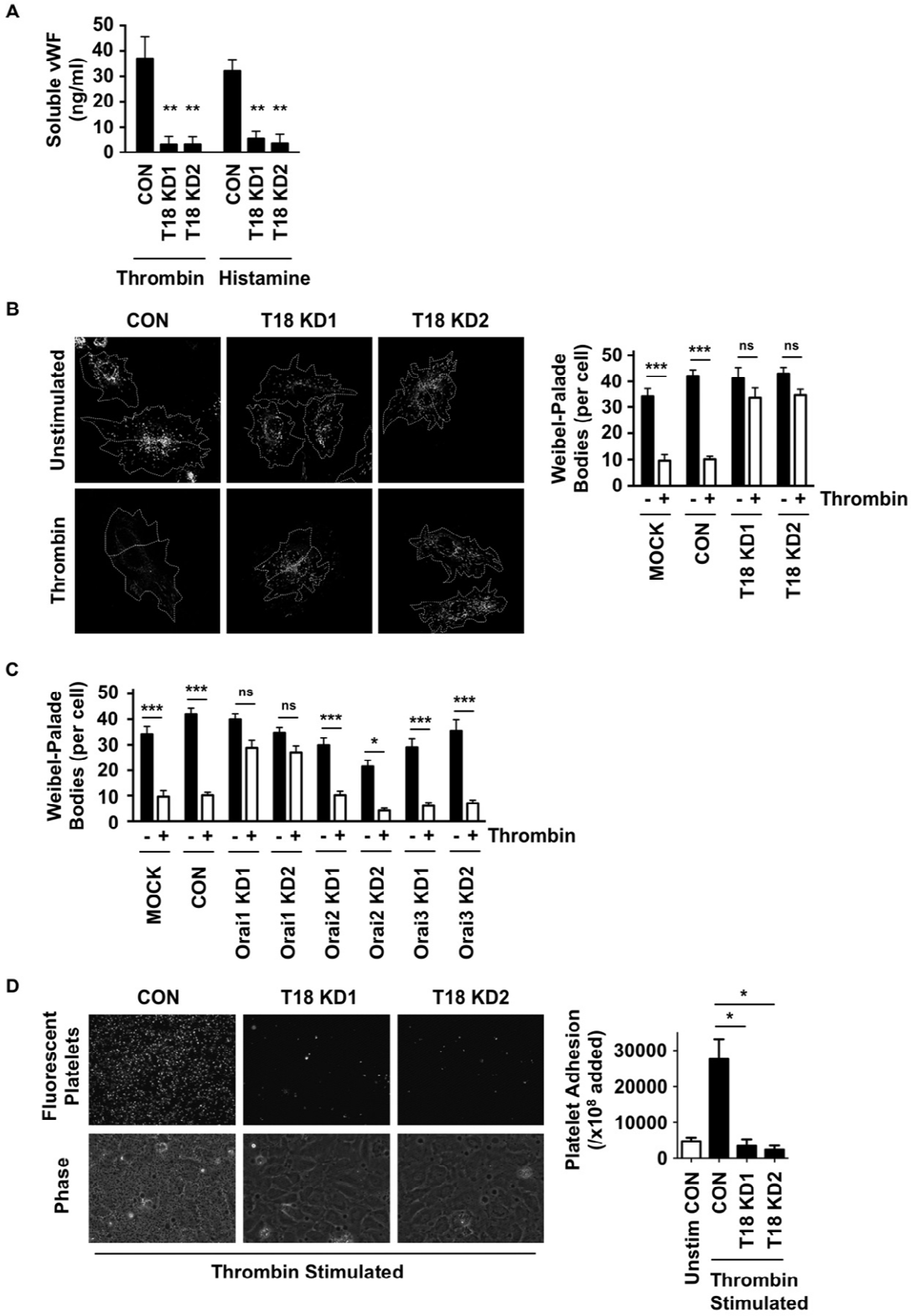
A
Soluble vWF (ng/ml)
50
40
30
20
10
0
** **
** **
CON
T18 KD1
T18 KD2
CON
T18 KD1
T18 KD2
Thrombin
Histamine
B
CON
T18 KD1
T18 KD2
Unstimulated
Thrombin
Weibel-Palade Bodies (per cell)
50
40
30
20
10
0
***
***
ns
ns
- + - + - + - +
Thrombin
MOCK
CON
T18 KD1
T18 KD2
C
Weibel-Palade Bodies (per cell)
50
40
30
20
10
0
*** *** ns ns *** * *** ***
- + - + - + - + - + - + - + - +
Thrombin
MOCK
CON
Orai1 KD1
Orai1 KD2
Orai2 KD1
Orai2 KD2
Orai3 KD1
Orai3 KD2
D
CON
T18 KD1
T18 KD2
Fluorescent Platelets
Phase
Thrombin Stimulated
Platelet Adhesion (/x10⁸ added)
30000
20000
10000
0
* *
Unstim CON
CON
T18 KD1
T18 KD2
Thrombin Stimulated

Figure 7. Tspan18-knockdown endothelial cells have impaired histamine- and thrombin-induced release of VWF. (A) HUVECs were transfected with a negative control siRNA (CON) or with one of two independent siRNAs targeting Tspan18 (T18 KD). 48 hours later, HUVECs were stimulated with 1 U/ml thrombin or 20 μM histamine for 5 minutes. Cultured media was removed and assayed for VWF by ELISA. Pre-stimulation levels of VWF were subtracted from these data. Error bars represent the standard error of the mean from three experiments (***P*<0.01). (B) HUVECs transfected as described in panel A were stimulated with 1 U/ml thrombin for 5 minutes, and the cells were fixed and stained with an anti-VWF antibody followed by Alexa488-conjugated secondary antibody. Representative confocal microscopy images are shown (left panels). Z-stack images were de-noised, background-subtracted and analyzed for the number of VWF cellular bodies, using ImageJ. Counts were made on five to ten cells per experiment for four independent experiments (right panel). Error bars represent the standard error of the mean (****P*<0.001 and ns denotes not significant). (C) The experiment and quantitation was conducted as for panel B, except HUVECs were mock-transfected with no siRNA (Mock), transfected with negative control siRNA (CON), or siRNA to Orai1, Orai2 or Orai3 (KD). (D) HUVECs were siRNA-transfected and simulated with 1 U/ml thrombin for 5 minutes as described in panel A. Human washed platelets were fluorescently labelled and incubated with the HUVEC monolayers. Non-adherent platelets were removed by washing and images were collected. Representative fluorescent images of adhered platelets (upper panels) and phase contrast images of the HUVEC monolayers and adhered platelets (lower panels) are shown, with quantitation of platelet adhesion from three independent experiments (right panel). Error bars represent the standard error of the mean (**P*<0.05).

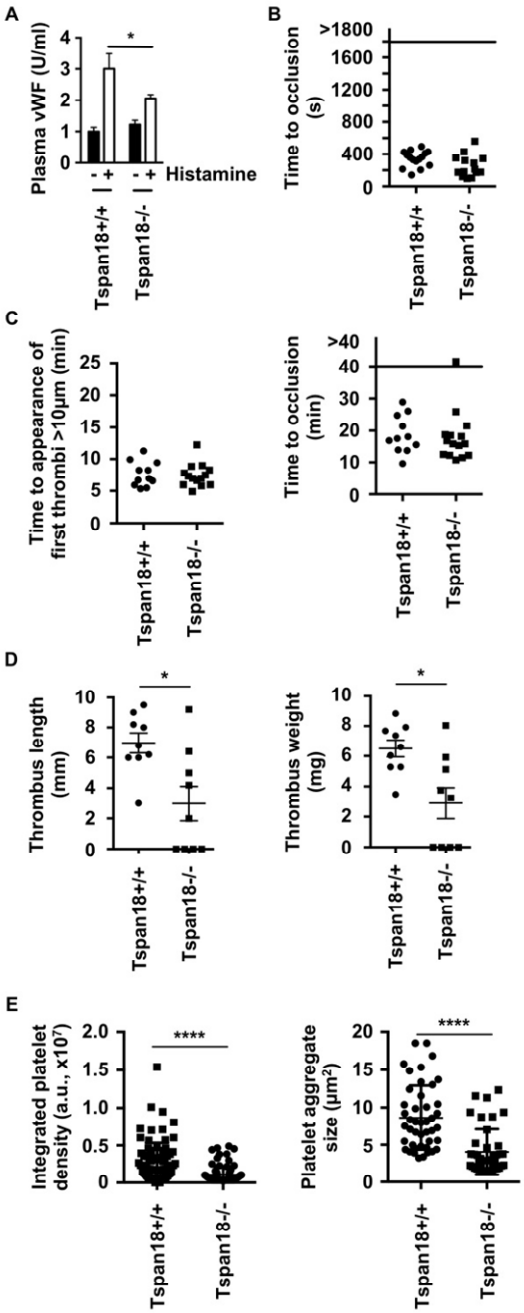
A
Plasma vWF (U/ml)
4
3
2
1
0
*
- + Histamine
- +
Tspan18+/+
Tspan18-/-
B
Time to occlusion (s)
>1800
1600
1200
800
400
0
Tspan18+/+
Tspan18-/-
C
Time to appearance of first thrombi >10µm (min)
25
20
15
10
5
0
Tspan18+/+
Tspan18-/-
Time to occlusion (min)
>40
40
30
20
10
0
Tspan18+/+
Tspan18-/-
D
Thrombus length (mm)
10
8
6
4
2
0
*
Tspan18+/+
Tspan18-/-
Thrombus weight (mg)
10
8
6
4
2
0
*
Tspan18+/+
Tspan18-/-
E
Integrated platelet density (a.u., x10⁷)
2.0
1.5
1.0
0.5
0
****
Tspan18+/+
Tspan18-/-
Platelet aggregate size (µm²)
20
15
10
5
0
****
Tspan18+/+
Tspan18-/-

Figure 8. Tspan18-knockout mice have impaired histamine-induced VWF release and impaired thombo-inflammatory responses. (A) Tspan18$^{+/+}$ and Tspan18$^{-/-}$ mice were intraperitoneally-injected with histamine and plasma VWF levels were measured 30 minutes later by ELISA. Error bars represent standard error of the mean from eight Tspan18$^{+/+}$ and seven Tspan18$^{-/-}$ mice (*P<0.05). (B) Tspan18$^{+/+}$ and Tspan18$^{-/-}$ mice were anaesthetized, the abdominal aorta exposed and mechanically injured through a single firm compression with forceps. Blood flow was subsequently monitored with a Doppler flowmeter to calculate the time until complete occlusion of the vessel. Each symbol represents one animal. (C) Tspan18$^{+/+}$ and Tspan18$^{-/-}$ mice were anaesthetized and the mesentery was exteriorized through an abdominal incision. Platelets were fluorescently labelled with Dylight 488-conjugated anti-GPIX derivative. Small mesenteric arterioles were exposed to $FeCl_3$-induced chemical injury via topical application. Time to appearance of the first thrombi was recorded (left panel), and the time until complete occlusion of the vessel was measured using fluorescence intravital microscopy (right panel). Each symbol represents one animal. (D) Tspan18$^{+/+}$ and Tspan18$^{-/-}$ mice were anaesthetized and surgery performed to stenose the inferior vena cava. After 48 hours, thrombus length (left panel) and weight (right panel) were measured. Each symbol represents one animal and error bars represent standard error of the mean (*P<0.05). (E) Myocardial ischemia-reperfusion injury was induced in the left ventricle of the beating heart of anaesthetized mice by occluding the left anterior descending artery for 45 minutes with a suture. Reperfusion was instigated for 2 hours by removal of the ligature, after which the organ was harvested. Frozen sections were analyzed for the presence of platelets by immunofluorescence microscopy. 3 litter-matched pairs of Tspan18$^{+/+}$ and Tspan18$^{-/-}$ mice were used, with 3 sections per mouse and 5 images analyzed per section. Each symbol represents one image. For each image, the integrated density value was calculated as a representation of the total number of platelets (left panel), and the average aggregate size was also calculated (right panel). Error bars represent the standard error of the mean (****P<0.0001). All data in this figure were analyzed by one-way ANOVA with Dunnett's multiple comparisons test.